

The CFHT Open Star Cluster Survey I – Cluster Selection and Data Reduction

Jasonjot Singh Kalirai¹

*Physics & Astronomy Department, 6224 Agricultural Road, University of British Columbia,
Vancouver, BC V6T-1Z1*

`jkalirai@physics.ubc.ca`

Harvey B. Richer¹

Gregory G. Fahlman^{1,2}

Jean-Charles Cuillandre²

Paolo Ventura³

Francesca D'Antona³

Emmanuel Bertin⁴

Gianni Marconi⁵

and

Patrick R. Durrell⁶

ABSTRACT

We present this paper in conjunction with the following as the first results in the CFHT Open Star Cluster Survey. This survey is a large *BVR* imaging data set of 19 open star clusters in our Galaxy. This data set was taken with the CFH12K mosaic CCD ($42' \times 28'$) and the majority of the clusters were imaged under excellent photometric, sub-arcsecond seeing conditions. The combination of multiple exposures extending to deep ($V \sim 25$) magnitudes with short (≤ 10 second) frames allows for studies ranging from faint white dwarf stars to bright turn-off, variable, and red giant stars. The

¹University of British Columbia

²Canada-France-Hawaii Telescope Corporation

³Osservatorio Astronomico di Roma

⁴Institut D'Astrophysique De Paris

⁵European Southern Observatory

⁶Penn. State University

primary aim of this survey is to catalogue the white dwarf stars in these clusters and establish observational constraints on the initial-final mass relationship for these stars and the upper mass limit to white dwarf production. Additionally, we hope to better determine the properties of the clusters, such as age and distance, and also test evolution and dynamical theories by analyzing luminosity and mass functions. In order to more easily incorporate this data in further studies, we have produced a catalogue of positions, magnitudes, colors, and stellarity confidence for all stars in each cluster of the survey. This reduction, along with the computed calibration parameters for all three nights of the observing run will encourage others to use this data in different astrophysical studies outside of our goals. Additionally, the data set is reduced using the new TERAPIX photometric reduction package, PSFex, which is found to compare well to other packages.

This paper is intended both as a source for the astronomical community to obtain information on the clusters in the survey and as a detailed reference of reduction procedures for further publications of individual clusters. We discuss the methods employed to reduce the data and compute the photometric catalogue. We reserve both the scientific results for each individual cluster and global results from the study of the entire survey for future publications. The first of these further publications is devoted to the old rich open star cluster, NGC 6819, and immediately follows this paper.

Subject headings: color-magnitude diagrams – open clusters and associations: general – methods: data analysis – techniques: photometric – white dwarfs

1. Introduction

The major effort in star cluster photometry has been directed towards globular clusters as they are some of the oldest structures in the Universe and can set a lower bound for the age of the Universe. These clusters were formed many billions of years ago and contain red, metal poor stars (Population II). Globular clusters can contain up to a million stars whereas the richest open clusters contain several thousands of stars at most. The stars in these less populated clusters are much bluer, younger, and metal rich (Population I) than the globular cluster stars. An in-depth analysis of these less crowded open star clusters is crucial to provide insight into the less well established theoretical stellar evolution models available for such clusters.

The present survey is a large *BVR* imaging data set of 19 open star clusters in our Galaxy. This data set was taken with the CFH12K mosaic CCD ($42' \times 28'$) and the majority of the clusters were imaged in excellent photometric, sub-arcsecond seeing conditions. There are very few other programs currently underway to address these issues, partly because a large field of view and a large telescope are required. Many papers have been published on individual open star clusters (some of which are in this survey), but the only major current survey similar to ours is the WIYN Open

Star Cluster Survey (WOCS). There are a few overlapping clusters in these two surveys however some of the science goals are different. The focus of the present study will not only include the measurement of key properties for most of the star clusters (such as age and distance), but will also test theoretical models by fitting isochrones. The ultimate goal of our survey is to catalogue the white dwarf stars for each cluster and constrain both the initial-final mass relationship for these stars and the upper mass limit to white dwarf production, both of which are currently rather poorly constrained by observational data (see Weidemann (2000) for a review).

The CFHT data for these clusters is unprecedented with regard to the diversity of the sample, the size of the data set, and the precision of the measurements. The sample of clusters, which span a large range of angular sizes, age, and metallicity values, were chosen on the basis of stellar density, age, and distance. Previous photometry on these clusters has been mostly limited to photoelectric and photographic observations, and usually concentrated on bright to intermediate magnitude ranges. The color-magnitude diagrams from these observations generally show a large amount of scatter both in the main-sequence and turn-off stars. The faintest stars recorded in most studies are ~ 17 - 18 th visual magnitude. While, the present photometry includes the bright end of the main sequence, the program is primarily intended to find white dwarf stars down to $V = 25$, and therefore provides some of the deepest images ever taken for open star clusters. A very well defined main sequence should be seen over a long magnitude range (10-12 magnitudes) for the rich, young clusters, which will allow for a wide range of investigations including main sequence termination, model fitting, and luminosity and mass functions. A small number of the clusters are very sparsely populated, but also among the youngest in the survey. These are especially important for white dwarf searches because any white dwarfs found in these clusters would have had to form from very massive progenitors, and therefore they will establish a constraint on the upper mass limit to white dwarf production.

Theoretical isochrones are commonly fit to observational results in order to validate the theory and/or determine the properties of the cluster. The lower main sequence often contains more scatter and errors due to photometric uncertainty for low signal to noise stars, so these isochrones have commonly been fit to the upper main sequence and turn-off only. The current data set goes fainter ($V \sim 25$) than the termination point of the main sequence for some of the clusters and will provide an excellent test to theoretical isochrones on the lower main sequence ($10 \leq M_V \leq 12$). Of particular interest is the change in slope of the main sequence caused by the various stages of stellar evolution and structure, such as the onset of H_2 dissociation-recombination in the stellar envelope at $(B-V)_0 = 1.0-1.1$, or the ‘kink’ in the main sequence at $(B-V)_0 = 0.3-0.4$ caused by changes from convective envelope models to radiative models. These slope changes will be used as guidelines for the fit of the observations with the theoretical models. The survey will use new up-to-date models calculated by the group at the Rome Observatory (Ventura & D’Antona, Private Communication).

In addition to model testing, there are many other scientific goals which we hope to complete with this data set. For example, a main sequence turn-on could potentially provide an independent

age measurement for some of the very young clusters for which the low mass stars have not yet reached the main-sequence. The faint magnitudes reached by such a study will also allow the study of white dwarf stars. Fitting models to the end of the white dwarf cooling sequence, if bright enough, will allow a third determination of the age measurement of some of the youngest clusters. For example, we use white dwarf cooling models (Richer *et al.* 2000) to determine that the white dwarf cooling sequence in an intermediate age cluster (~ 250 Myrs) will terminate at $M_V \sim 11.2$, depending on the mass of the stars, whereas for a much older cluster (~ 2 Gyrs), the end of the cooling sequence occurs at a significantly fainter magnitude of $M_V \sim 13.5$. Therefore, even for a moderately close cluster, the depth of the current photometry should allow us to establish the white dwarf cooling age for a large number of the clusters in the survey (see Table 1). For the older clusters for which the termination of the white dwarf cooling curve is fainter than our limiting magnitude, we should nevertheless be able to identify a significant number of white dwarf candidates above our mean cut off of $V \sim 25$. Other studies that will be looked at involve producing luminosity and mass functions for these clusters. In particular, these will be explored for evidence of dynamical evolution in the older clusters. An updated mass-luminosity relation from new stellar models will also be used to test mass segregation in the clusters by comparing the mass functions for various annuli at different distances from the centers of the clusters. This test will be possible for a wide range of masses ($\sim 0.5 - 4M_\odot$) for most of the intermediate aged clusters. Improved distance estimates of the clusters will be found by establishing a fiducial of the main sequence and comparing to the Hyades main-sequence which has a very well established distance from Hipparcos measurements (Perryman *et al.* 1998). Chemical evolution theories for old stars in the clusters will be tested by comparing the masses of white dwarfs to their progenitors on the main-sequence. Number counts involving the red giant/white dwarf ratio will be carried out by assuming conservation of star number through various stages during stellar evolution, to establish the number of expected white dwarfs. Binary star tests will be undertaken to determine the population of binaries (relative to main-sequence stars) in each cluster. These have been shown to have important evolutionary effects, especially for the younger, less dense clusters (de la Fuente Marcos 1996).

Additionally, since most of these clusters are confined to the disk of the Galaxy, this work allows for a better understanding of the dynamical evolution of the Galactic disk as well as the Galactic star formation history.

Our photometric catalogue has been produced in order to encourage and expedite studies outside the scope of our goals. The current paper will introduce these clusters and the specific photometry for each one. Answering the questions raised above will be reserved for a cluster-by-cluster analysis and will be presented in subsequent papers as a part of the CFHT Open Star Cluster Survey. The first of these papers, entitled ‘The CFHT Open Star Cluster Survey II : Deep CCD Photometry of the Old Open Star Cluster NGC 6819’, immediately follows this paper.

2. Observations

The data for these 19 clusters (see Table 1) was taken during an excellent three night observing run with the Canada-France-Hawaii Telescope (CFHT) on October 15-18th 1999, using the new CFH12K camera. The optical detector is a 12,288 by 8,192 pixel CCD mosaic camera for high resolution wide field imaging at the CFHT prime focus. This mosaic camera is the largest close-packed CCD currently being used for astronomical research. The CCD camera was ideal for our purposes as it covers a large area on the sky (42 by 28 arc-minutes, or about 1.5 times the area of the full moon), and also contains a large number of pixels ($\geq 10^8$) to ensure a high angular sampling. The camera is equipped with twelve 2048 \times 4096 pixel CCDs with an angular size of 0.206 arc-seconds per pixel at the f/4 prime focus. The orientation of the CCDs within the mosaic is such that chips 00-05 form a sequence on the bottom row from left \rightarrow right, and chips 06-11 are directly on top of the bottom row. Therefore the inner 4 CCDs are chips 02, 03, 08 and 09, and the outer 4 CCDs are chips 00, 05, 06 and 11.

Data for each cluster was taken in three filters: B, V and R. The R images were usually rather shallow and are used to provide some leverage for the reddening of the clusters based on color-color diagrams. The optimal exposure time to be used was determined so as to achieve a limiting magnitude 1 magnitude fainter than the oldest expected white dwarfs in most of the clusters. This was found by equating the cluster age to the white dwarf cooling time (Richer *et al.* 2000). For a few of the older clusters (such as NGC 6819), it was not feasible to try and observe the end of the white dwarf cooling sequence from ground based imaging as it was expected to be too faint, so we hope to detect as many white dwarfs as possible above our limiting magnitude.

To achieve a higher signal to noise ratio, multiple 300 second exposures were taken for some of the clusters in both the V and B filters. Additionally, single 50 and 10 second exposures were obtained in all three of the B, V, R filters. The long exposures in each band were dithered from one another to prevent a star from landing on a bad pixel in more than one frame. The multiple fields were averaged and combined together using the FITS Large Images Processing Software (FLIPS) (see section 3.1). In many cases the CFH12K images for these clusters are the deepest yet, and indicate a much richer cluster population than previously thought. The images also provide a more complete aerial coverage for each of the clusters than most previous studies. In addition to these frames, several flat-field images and bias frames were also taken (see section 3). Five of the clusters in our sample have sizes that exceed that of the CCD mosaic field of view, and thus additional images of neighboring blank fields were also taken. These will be used for background subtraction by obtaining an estimate of the number of field stars in the region around the cluster. Table 2 summarizes the observational data that was taken for each cluster in the survey, as well as other relevant information pertaining to the exposures.

Since most of these clusters have not been extensively studied in the past it is difficult to compare results with ‘good’ previous photometry. Furthermore, none of the clusters contain any well established standard stars in the field. These factors lead to the critical calibration stage of

the reduction which we address by taking multiple images of the SA-92 and SA-95 standard star fields (Landolt 1992). Calibration is further discussed in section 5, where we provide details of numbers of stars/chip used to calibrate the data set (see Tables 2 & 3 for particulars).

3. Data Reduction

The data for the survey was reduced and organized locally at CFHT. The first stages of the reduction involve pre-processing the raw data as shown in equation (1). First several zero exposure bias frames are taken and subtracted from the images (de-biasing) to account for counts read out even if no light falls on the CCD. A dark current is also subtracted from the longer exposures. After the images are de-biased, the data is flat-fielded to account for pixel-to-pixel variations. For the flat-field frames, we combined twilight flats taken from all three nights of the observing run.

$$Preprocessed\ Frame = \frac{raw\ image - bias}{flat - bias} \quad (1)$$

3.1. FLIPS

3.1.1. Pre-processing

FITS Large Images Processing Software (FLIPS) is a highly automated software package developed at CFHT (Cuillandre 2001). FLIPS was originally developed for early CCD mosaic wide field imagers at CFHT, such as MOCAM (4k × 4k pixels, 1994) and UH8k (8k × 8k pixels, 1995), but has now been updated and upgraded with new functions to handle CFH12K images. This software is ideal for our survey as it is optimized for both speed and requires limited memory resources. FLIPS is not a photometric reduction package and should be thought of as a package which performs similar functions to the commonly used IRAF task **mscred**.

FLIPS is designed to operate on individual chips within the CFH12K mosaic. The first steps involve averaging the ‘good’ exposures for each of the bias, dark and flat exposures. For each filter, these exposures can be accepted or rejected based on the on-screen statistics (ie. if image level is too high (saturation) or too low (no flux)). The flats used in the survey are twilight exposures averaged and sigma clipped (iteratively eliminating if ±sigma cut is not satisfied) from all three nights of the run, whereas the darks were combined by taking a median from a sigma clipped sample. FLIPS will then search through all the images for each cluster and apply the above corrections (bias, dark, flat) based on input parameters specific to the CCD and data. These detailed parameters for each of the operations have been optimized to produce the best processing. One of the important features of FLIPS is that it normalizes the background sky value to the chip with the highest sky value (lowest gain), CCD 04. This provides for a scaled data set with a smooth background on all chips. Therefore, the instrumental zero points for the data set will all be almost equal. The final processed data show very small variations from a completely smooth background. By measuring

the statistics in small boxes of size comparable to the mean stellar aperture size at various positions in the mosaic, we find the flat-fielding to be good to $\sim 0.5\%$ in V and $\sim 0.7\%$ in B, averaged over $11''$ sq. patches.

3.1.2. Combining Multiple Exposures

In order to achieve a higher signal to noise ratio and a deeper color-magnitude diagram, we obtained several deep exposures for some clusters. These exposures were dithered from one another (see section 2) and then aligned and combined into one image. We use a program called **align**, within FLIPS, which searches through a specified area on each CCD and finds patterns of common stars based on both the positions and fluxes of the stars. This pattern recognition algorithm works very quickly for moderately rich clusters, however it is quite slow for sparse fields. FLIPS **align** uses SExtractor (Bertin & Arnouts 1995) to create an X Y catalogue of aperture magnitudes and positions which **align** searches through to find the geometric patterns. This catalogue does not contain the final photometry as these magnitudes are only used for this one purpose. An important aspect of **align**, as we will shortly see, is that it defines the true sky background and atmospheric transmission across the data set. Next we invoke the **imcombred** command within FLIPS to register the frames with respect to one common image, and average the data. The parameters for the variable transmission (if present) and sky background are taken and applied directly from the **align** output. **Imcombred** re-centers the individual images based on the X & Y offsets derived for each CCD. For a given pixel coordinate, a column of pixels from each of the individual images is created with the proper background and transmission corrections. Then a CCD sigma clipping of ± 5 is applied on that set of pixels to determine the exact shifts. This requires a determination of the readout noise and gain to evaluate properly the expected noise in the signal and reject outliers.

We found that the point-spread-function fit to the stars was being skewed in the average because the centers of stellar positions were not being located accurately enough. In order to correct the problem, we use a FLIPS **imcombred** option called sub-pixelling. This sub-pixelling parameter can be given a value of $n = 1, 3$ or 5 , and will split each CFH12K pixel ($0''.206$) into n^2 boxes, and then locate the center within each of these sub-divisions. This procedure is similar to the **drizzle** technique in IRAF and works to better align the stellar profiles directly on top of one another in the above combining procedures. The sub-pixelling feature within FLIPS also maintains the original resolution of the image and does not lose any spatial information in the combining process. The resulting CMD (for $n = 5$) was also found to go about 0.3 magnitudes fainter, thereby indicating that the additional step allowed for the measurement of lower signal to noise objects. This division led to a very slow computing process of averaging the frames (as expected for 2.5 billion pixels on each mosaic), however the results were excellent.

The resulting data images are next used in the TERAPIX PSF-extraction and modelling tool, PSFex, to find magnitudes, colors, errors, and stellarity.

4. PSFex

Point-Spread-Function Extractor (PSFex) is a highly automated program which will be integrated in the code of the next SExtractor version (Bertin, Private Communication). SExtractor detects sources through a segmentation process consisting of 6 essential steps: estimation of the sky background, thresholding, deblending of overlapping images, filtering of the detections, photometry, and star/galaxy separation. Further details and simulation results are given in Bertin & Arnouts (1995). SExtractor is most commonly used to distinguish between stars and galaxies at faint magnitudes by assigning a stellarity index to the objects. This process also eliminates bad pixels caused by cosmic ray hits. The stellarity is key to our project as white dwarf stars and faint star forming galaxies both appear as faint, blue objects. SExtractor determines the stellarity of objects by computing a neural network (a group of connected units) which learns based on other (high signal to noise) stars in the field. The classification is highly dependent on the seeing of the image and generally will be less accurate for faint stars than faint galaxies because of crowding: faint stars have a higher probability of catching wings added to the profile by a background galaxy which would result in misclassification. The shape of all diagrams (stellarity vs. magnitude) that we produced using SExtractor agree with that of the Monte Carlo experiments executed during the tests of the package by Emmanuel Bertin. Furthermore, our results seem to indicate that a simple constant magnitude stellarity cut (0.95 is commonly used) may not be a real indication of the separation of stars from galaxies. We find a common pattern in the stellarity vs. magnitude diagram for all rich clusters, and this may be a more accurate indication of the separation between the galactic and stellar sequences. The above points are illustrated in Figure 1, for the stars of the young, rich open cluster NGC 2099. This type of cut would have to be used with caution however as there are some objects that fall under the line, yet are brighter and have a slightly higher stellarity than sources that are over the line. More data will eventually allow us to decide on an optimal stellarity cut.

PSFex automatically creates a PSF based on a set of bright, unsaturated and isolated stars. Included in the PSF are polynomial basis functions which can map the variations of the PSF across the field. This is done immediately after the SExtractor find catalogue is created. Next, it uses this PSF to derive PSF magnitudes and colors for the objects in the original catalogue. This entire process is not very computer intensive and is easily executed with very little user interaction.

For the CFHT Open Star Cluster Survey, we have chosen to use a variable PSF for all fits to account for small changes in the profiles of stars over the large range of each CCD. Additionally, there are differences between each of the 12 CCDs on the mosaic so the analysis is done on a single chip basis for all exposures. Preliminary results, based on the differences in measured magnitudes of PSFex and ALLSTAR (Stetson 1992), the shape of the main-sequence in PSFex compared to ALLSTAR, and the number of stars that were measured indicate consistency between the two packages. To better illustrate the small scatter measured for common stars in these two packages, we show a comparison of the difference in magnitudes vs magnitude for the two packages in Figure 2. Results on other CCDs and other frames were all much better than this, some by several factors.

A photometric error bar (combining errors from both programs) is also shown in order to judge the agreement between the two systems. The spread ($2/3\sigma$) is within the errors along the tight vertical sequence of stars, except at the very bright and faint ends. The scatter at the bright end is in part due to saturation and also due to the handling of blended objects in the frames. Although the low end scatter may also appear to be larger than the errors this may be simply due to different detection parameters between the two packages. Our expected limiting magnitude is indicated on Figure 2. The results for different magnitude cuts, in the form of a histogram, are also shown in Figure 3. The distribution peaks strongly at $\Delta B = 0$ and quickly falls off indicating a very small amount of scatter in all but the very faint case (see lower right diagram).

5. Calibration of Instrumental Data

5.1. Landolt Standard Stars

Observations of Landolt (1992) standard stars in SA-92 and SA-95 were obtained in order to convert the instrumental magnitudes to real magnitudes as shown in equations (2) and (3). We use a total of 23 calibration frames of different exposure times, air-masses, and wavelength filters to transform the data from instrumental magnitudes to calibrated magnitudes. Table 2 provides information on the number of exposures for each frame, on each night.

$$v_{instr} = V + \alpha X + \beta(B - V) + Z_v \quad (2)$$

$$b_{instr} = B + \alpha' X + \beta'(B - V) + Z_b \quad (3)$$

In these equations v_{instr} and b_{instr} are instrumental magnitudes (discussed more later). For equation (2), α is the coefficient of the air-mass term X , β is the coefficient of the color correction term $(B-V)$, and Z_v is the zero point shift for the V-band. Similarly, in equation (3), b_{instr} , α' , β' , and Z_b are the corresponding parameters for the B-band images. There are systematic differences between chips on the CCD so separate calibrations are required for each chip. The color term does not change with different exposures or nights of observations. The zero points are the most critical part of this first stage of the calibration equations. This shift tells us the relationship between the instrumental magnitudes and the real magnitudes, taking the exposure time into account.

The magnitudes of the standard stars used by Landolt are based on non-linear transformations of the magnitudes and colors of the stars in several different filter bands. The final magnitudes derived for the stars are based on the total amount of flux that the star emits. However, the fitting parameter used in our PSF photometry is one that maximizes the signal to noise ratio. In order to collect the entire light from the star without an increase in the background level, we use aperture photometry for calibration. For those stars which are not saturated and appear in both Landolt's

paper (Landolt 1992) and our images of SA-92 and SA-95, we use DAOPHOT to produce a curve-of-growth of flux for aperture sizes ranging from 8 to 20 pixels. At an aperture size of 16 pixels it is found that the magnitude begins to level off (less than 0.01 magnitude difference in all cases). Therefore, an aperture size of 16 pixels collects almost all of the light from the star ($\geq 99\%$). For these stars we use the flux from this aperture in our calibration equations.

To prevent Landolt (1992) objects from being saturated on our images, we choose extremely short exposure times depending on the filter. The number of exposures that were used in the calibration for each night is summarized in Table 3.

The calibration parameters are found by using a least squares method to determine the coefficients of the air-mass, color and zero point terms. The specific algorithm is based on a method designed by Harris (Harris, Fitzgerald & Reed 1981). These parameters are solved for in those chips which contained enough calibration stars for the calibration program to produce accurate (low sigma) results. The chips with only a few or no calibration stars do not help this analysis. Some sections of Landolt’s frames were highly concentrated with calibration stars however, the CFHT chips did not align with these regions when the calibration frames were taken. It would be strongly preferred to have enough calibration stars in each chip to get accurate parameter values, which could then be used individually. Additionally, dithering the calibration frames could have allowed for the measurement of common standards on different chips, which would also help in better constraining individual CCD calibration parameters. We are forced to average the ‘good’ chips (02,04,07,08) together and use the resulting parameters on other chips. There is minimal scatter in the parameters for different chips so this method is reliable. For example, the photometric uncertainty in the zero points for the standard stars on all four chips during night 1 of the observing run were measured to be ~ 0.015 in V and ~ 0.014 in B. The air-mass coefficients were determined to be 0.088 ± 0.01 in V and 0.165 ± 0.005 in B, both in good agreement with CFHT estimations of 0.10 and 0.17 respectively. The color terms were averaged over the three night observing run and are in agreement with CFHT estimations in the V filter and slightly lower than estimations for the B filter. Similar estimates are also obtained for night 2, whereas for night 3 there are too few observed standards to establish low sigma calibration parameters. Therefore, we use the transformation equations from night 1 and 2 to create more standards and then apply these to the night 3 data. These results were also within the errors given above.

To illustrate the small scatter between the actual magnitude of each standard star, and the calculated value from the least squares solution, we present a composite O-C diagram in Figure 4. There is clearly no obvious bias in this diagram, which includes all calibration stars on all nights, in all bands. O-C diagrams for data in each of the separate V and B filters, individual nights of the observing run, or red vs. blue segregation also shows no trends or biases. The small vertical spread is caused by measurements of the same star at various air-masses and/or exposure times.

5.2. On-Field Standards

As mentioned earlier, we have determined all of the best fit calibration parameters in both the V and B filters. One can now simply use these in equations (2) and (3) to determine a preliminary zero point term. Next, we find Z'_v and Z'_b , which are denoted in equations (4) and (5) as the final shifts of the instrumental magnitudes to the calibrated magnitudes, by creating on-field standards on the science frames. These new zero points will include the correction needed in going from aperture to PSF magnitudes. The stars that are used for this are isolated and bright, yet non-saturated. Finally, equations (2) and (3) are solved for $V + \beta(B - V)$ and $B + \beta'(B - V)$ which are then used in equations (4) and (5), along with the PSF magnitude values to derive Z'_v and Z'_b for each chip. These new zero points can be used to calibrate the entire data set to calibrated magnitudes as they are particular to the science frames only. This shift is employed by first solving the calibration equations for a color term, as shown in equation (6), and then applying the color term to equations (4) and (5) to get the V and B magnitudes. This method can be used for all clusters in the survey by using the determined calibration parameters for the night in which the respective cluster was imaged.

$$V = v_{PSF} - Z'_v - \beta(B - V) \quad (4)$$

$$B = b_{PSF} - Z'_b - \beta'(B - V) \quad (5)$$

$$B - V = (1 + (\beta' - \beta))^{-1} [(b - v)_{PSF} - (Z'_b - Z'_v)] \quad (6)$$

6. Results

At the current time, we have completed reductions for two clusters in the survey, NGC 2099 and NGC 6819, and have begun reducing two additional clusters. These clusters are both relatively rich in stellar content, though they are quite different in age. Following this paper we present a separate paper of complete results on NGC 6819 (Kalirai *et al.* 2001). This will shortly be followed with the analysis of NGC 2099, at which time we will start evaluating the clusters based on a pre-determined priority system. The results for NGC 2099 and these other clusters will include white dwarf star analysis, white dwarf cooling ages, isochrone fitting, statistical subtraction of field stars, luminosity and mass functions, and binary star studies.

7. Conclusion

We have determined the instrumental magnitudes for the entire CFHT Open Star Cluster Survey. Soon, we will make this photometric catalogue available for general studies. The catalogue will consist of positions, magnitudes, colors, and stellarity for the 19 open star clusters in the survey. Preliminary results and color-magnitude diagrams for four of the star clusters that we have looked at indicate a strong potential for successful completion of the global goals of the survey:

- 1.) Constraining the initial-final mass relationship for white dwarf stars in these clusters.
- 2.) Establishing observational constraints to the upper mass limit to white dwarf production.
- 3.) Refining parameters, such as age and distance, for the clusters.
- 4.) Testing up-to-date theoretical models.
- 5.) Investigating evolutionary processes in the cluster by exploring the luminosity and mass functions.

The rich stellar content of these clusters, large aerial coverage, and the excellent photometry, allows for a large range of astronomical studies outside of our goals: the study of bright variable stars in open cluster, core-overshooting constraints for turn-off stars, astrometric studies etc... The results for NGC 6819, the first detailed studied cluster in the survey follow in the next paper.

REFERENCES

- Abt, H.A., Bolton, C.T., and Levy, S.G. ApJ, 171, 259.
- Auner, G., 1974, A&AS, 13, 143.
- Barbon, E.R. and Hassan, S.M., 1974, A&AS, 13, 293.
- Becker, W. and Svolopoulos, S., 1976, A&AS, 23, 97.
- Bertin, E. and Arnouts, S., 1995, A&AS, 117, 393.
- Burkhead, M.S., 1971, AJ, 76, 3, 251.
- Claria, J.J., Piatti, A.E., and Lapasset, E., 1998, A&AS, 128, 131.
- Claria, J.J., 1972, AJ, 77, 868.
- Cudworth, K.M., 1972, A&A, 18, 318.
- Cuffey, J. and McCuskey, S.W., 1956, ApJ, 123, 59.
- Cuillandre, J-C., 2001, A&A, In preparation.

- de la Fuente Marcos, R., 1996, *A&A*, 314, 453.
- Foster, D.C., Theissen, A., Butler, C.J., Rolleston, W.R.J., Byrne, P.B. and Hawley, S.L., 2000, *A&AS*, 143, 409.
- Galadi-Enriquez, D., Jordi, C. and Trullols, E., 1998, *Ap&SS*, 263, 307.
- Garcia-Pelayo, J.M. and Alfaro, E.J., 1984, *PASP*, 96, 444.
- Harrington, P. 1992, *S&T*, 83, 464.
- Harris, W.E., Fitzgerald, M.P. and Reed, B.C., 1981, *PASP*, 93, 507.
- Hill, G. and Barnes, J.V., 1971, *AJ*, 76, 110.
- Hogg, A.R. and Kron, G.E., 1955, *AJ*, 60, 365.
- Ianna, P.A. and Schlemmer, D.M., 1993, *AJ*, 105, 209.
- Jeffries, R.D., 1997, *MNRAS*, 292, 177.
- Jones, B.F. and Prosser, C.F., 1996, *AJ*, 111, 1193.
- Kalirai, J.S., Richer, H.B., Fahlman, G.G., Cuillandre, J., Ventura, P, D’Antona, F., Bertin, E., Marconi, G., and Durrell, P., *AJ*, submitted.
- Lattanzi, M.G., Massone, G. and Munari, U. 1991, *AJ*, 102, 177.
- Landolt, A. U., 1992, *ApJ*, 104,340.
- Lindoff, U., 1972, *A&AS*, 7, 497.
- Maitzen, H.M., 1993, *A&AS*, 102, 1.
- Marie, M.A., 1992, *Ap&SS*, 198, 121.
- Menzies, J.W. and Marang, F., 1996, *MNRAS*, 282, 313.
- Mermilliod, J.C., Huestamendia, G., del Rio, G., Mayor, M., 1996, *A&A*, 307, 80.
- Penia, J.H. and Peniche, R., 1996, *RMAA*, 32, 193.
- Penia, J.H. and Peniche, R., 1994, *IAUS*, 162, 303.
- Perry, C.L, Lee, P.D. and Barnes, J.V., 1978, *PASP*, 90, 73.
- Perryman, M.A.C., Brown, A.G.A., Lebreton, Y., Gomez, A., Turon, C., de Strobel, G.C., Mermilliod, J.C., Robichon, N., Kovalevsky, J. and Crifo, F.,1998, *A&A*, 331, 81.
- Prosser, C.F. and Giampapa, M.S. 1994, *AJ*, 108, 964.

- Prosser, C.F. 1993, *AJ*, 105, p.1441.
- Reimers, D. and Koester, D., 1994, *A&A*, 285, 451.
- Richer, H.B, Hansen, B., Limongi, M., Chieffi, A., Straniero, O., Fahlman, G.G., 2000, *ApJ*, 529, Issue 1, 318.
- Rosvick, J.M. and VandenBerg, D., 1998, *AJ*, 115, 1516.
- Sagar, R., 1976, *Ap&SS*, 40, 447.
- Sanders, W.L., 1973, *A&AS*, 9, 213.
- Sanders, W.L., 1972, *A&A*, 19, 155.
- Sanders, W.L. and van Altena, W.F., 1972, *A&A*, 17, 193.
- Sanner, J., Altmann, M., Brunzendorf, J. and Geffert, M. 2000, *A&A*, 357, 471.
- Schneider, H., 1987, *A&AS*, 71, 531.
- Stetson, P.B., 1992, ‘Further Progress in CCD Photometry,’ in *Stellar Photometry – Current Techniques and Future Developments*, IAU Coll. 136, eds. C.J. Butler and I. Elliot, p.291.
- Sung, H. and Bessell, M.S., 1999, *MNRAS*, 306, 361.
- Tian, K.P., Zhao, J.L., Shao, Zh.Y., Stetson, P.B., 1998, *A&AS*, 131, 89.
- Turner, D.G. 1992, *AJ*, 104, 1865.
- Ungren, A.R., 1966, *ApJ*, 71., 08.
- Ventura, P. and D’Antona, F., Private Communication.
- Weidemann, V. 2000, *A&A*, 363, 647.
- West, F.R. 1967, *ApJ*, 14.

Fig. 1.— The star/galaxy classification from SExtractor seems to indicate two sequences (split by the line), where the top sequence may be indicative of stars and the bottom of galaxies.

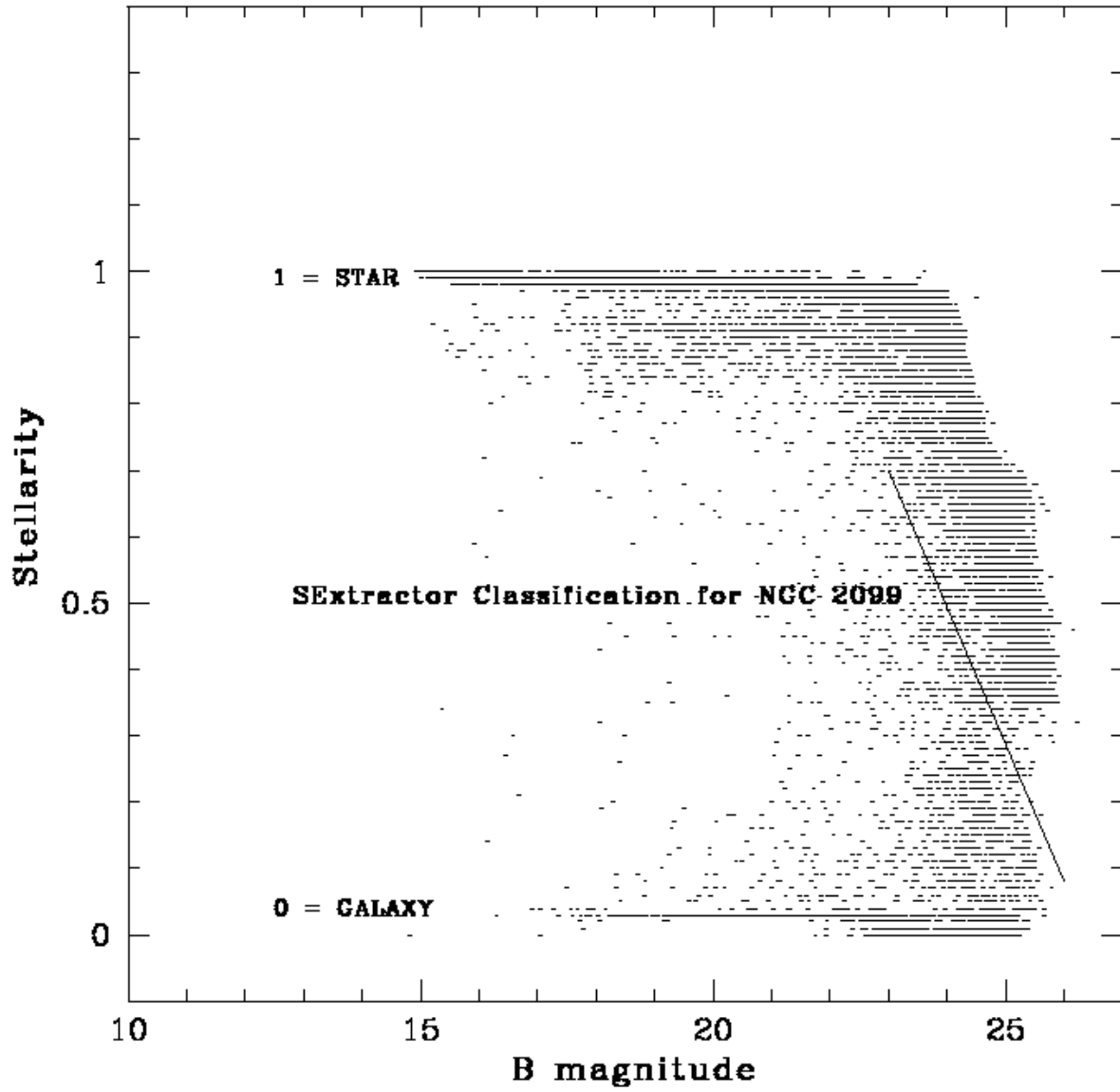


Fig. 2.— A comparison of PSFex magnitudes with ALLSTAR magnitudes indicates good agreement between the two packages within the errors. A very small bias is seen at faint magnitudes ($B \geq 25$) which is fainter than our limiting magnitude cut-off. The bias effect on other CCDs and in other filters was less than that shown here.

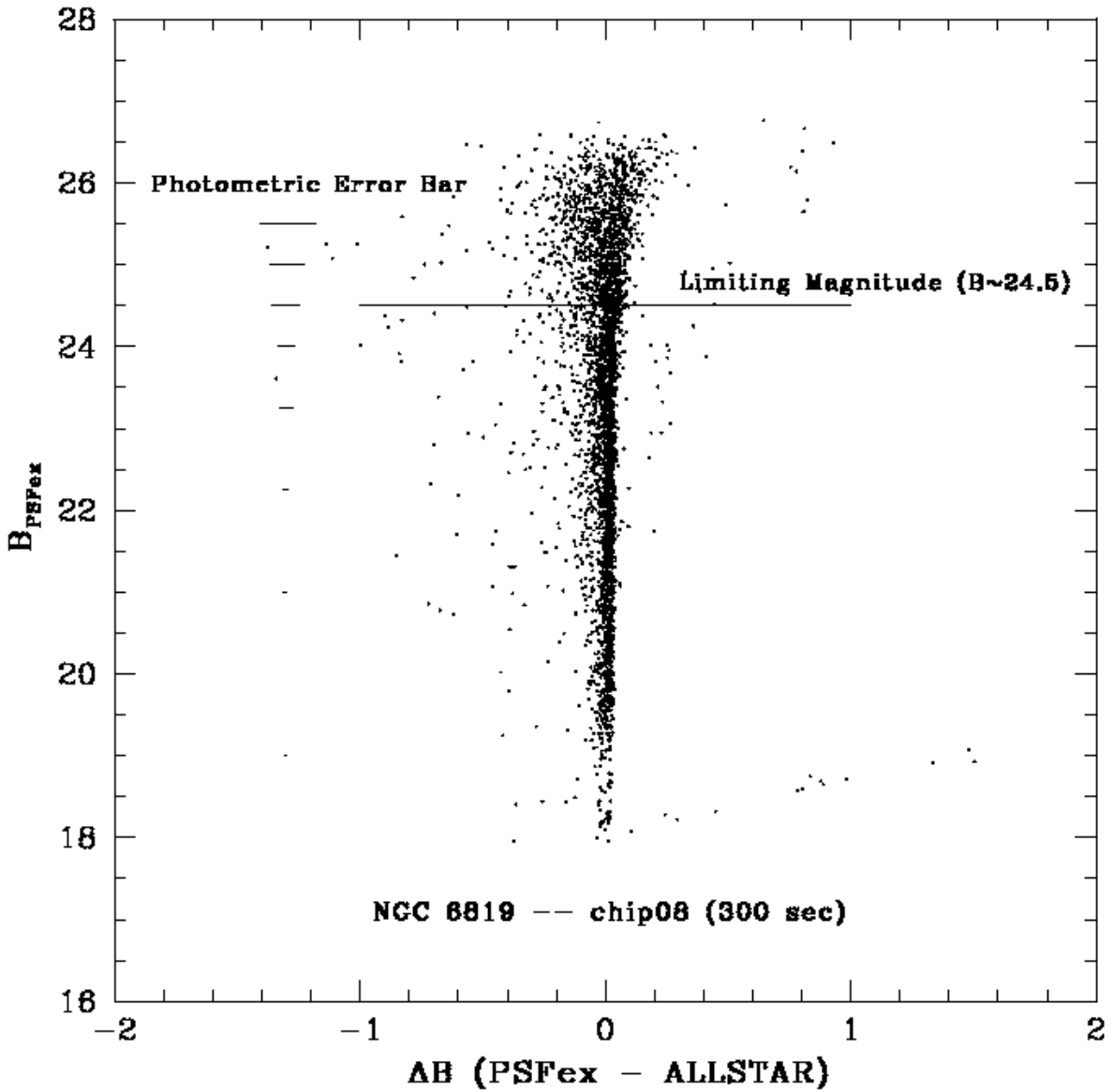


Fig. 3.— Histograms for different magnitude cuts show a large pile up of stars with $\Delta B = 0$ in the PSFex - ALLSTAR plane. The spread in the data is small for all but very faint objects.

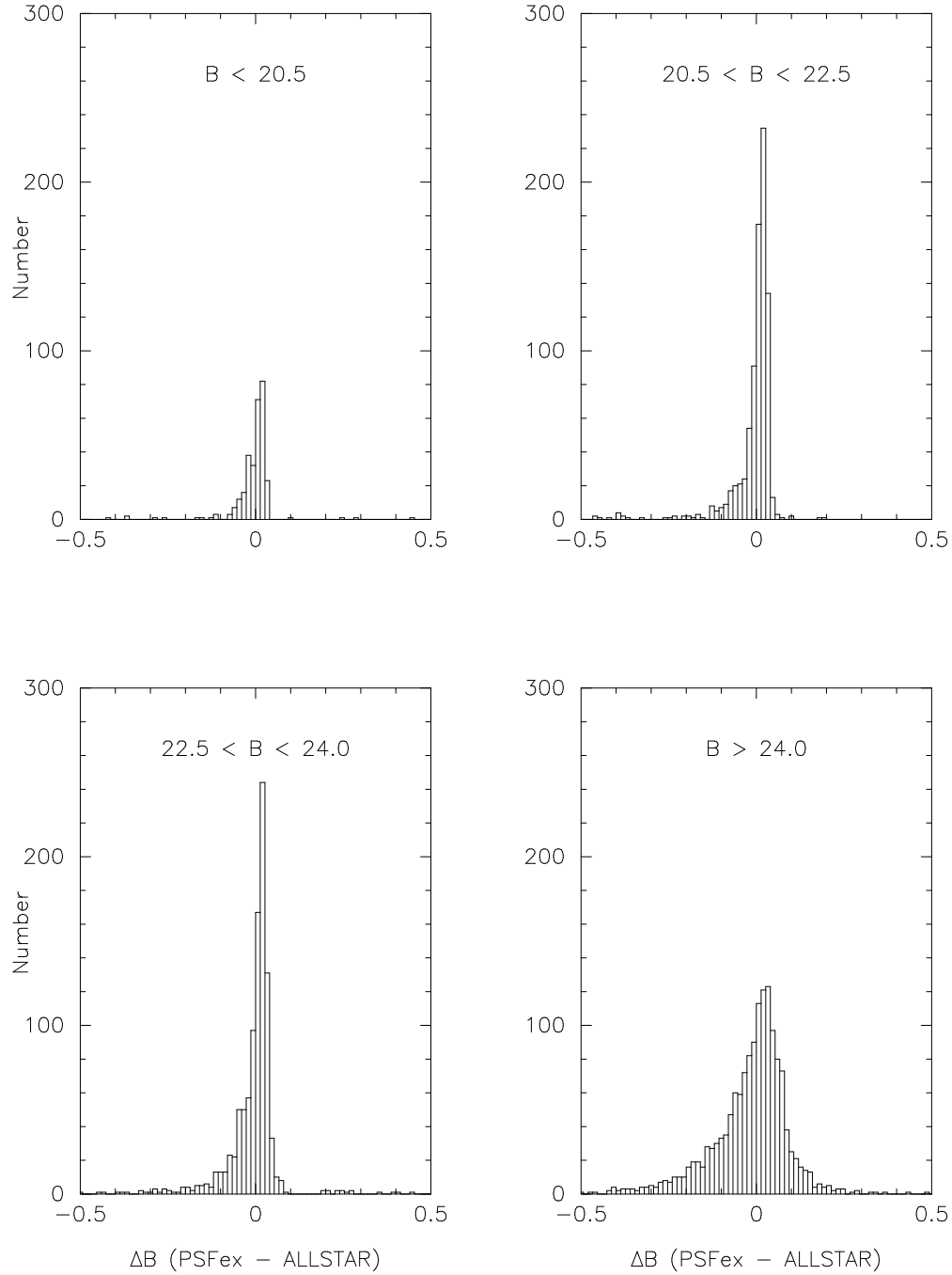


Fig. 4.— An O-C diagram for calibration stars on all three nights, and in both the V and B filters shows no biases or trends. The small vertical spread is caused by slightly different measurements of common stars at different air-masses and/or exposure times.

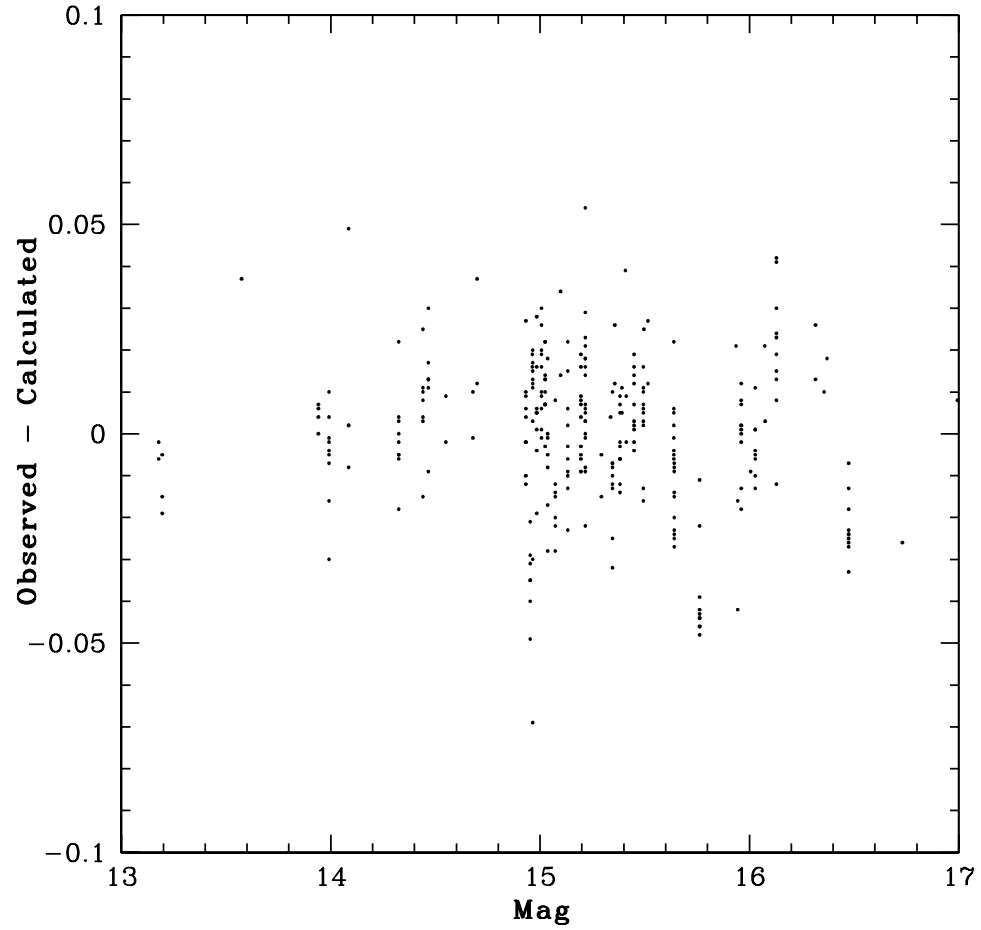


Table 1. The CFHT Open Star Clusters

Cluster	α (1950)	δ (1950)	Night	Log(Age)^1	$(m-M)_V^1$	$E(B-V)^1$	Angular Size ($'$) ¹	References
NGC 1039 (M34)	2 38.8	42 34	1	8.26	8.82	0.10	35	1,2
NGC 2323 (M50)	7 00.8	-8 16	1	8.05	10.73	0.23	16	3,4
NGC 6633	18 25.3	6 32	1	8.66	8.43	0.16	27	5,6,7
NGC 1342	3 28.4	37 10	1	8.71	9.46	0.26	14	...
NGC 2343	7 05.9	-10 34	1	7.36	10.19	0.15	7	8,9
NGC 6819	19 39.6	40 04	1	9.3	12.3	0.16	8	10-14
IC 4665	17 43.8	5 44	2	7.58	8.29	0.19	≥ 30	15-20
NGC 1778	5 04.7	36 59	2	8.05	11.93	0.34	7	21,22
NGC 225	0 40.5	61 31	2	8.23	9.74	0.24	12	23
STOCK 2	2 11.4	59 02	2	8.23	8.62	0.38	≥ 30	24
NGC 1647	4 43.1	18 59	2	8.22	9.85	0.41	45	25
NGC 1960 (M36)	5 32.8	34 06	2	7.5	11.25	0.22	12	26
NGC 2301	6 49.2	0 31	2	8.19	9.79	0.04	12	27,28
NGC 1750	5 00.9	23 35	2	8.30	10.08	0.34	≥ 20	29,30
NGC 2099 (M37)	5 49.1	32 32	2	8.6	11.8	0.28	26	31-34
NGC 7243	22 13.3	49 38	2	7.9	10.11	0.24	21	35
NGC 2169	6 05.6	13 58	3	7.18	10.67	0.19	7	36-40
NGC 2251	6 32.0	8 24	3	8.31	11.26	0.22	10	...
NGC 2168 (M35)	6 05.8	24 21	3	8.05	10.44	0.25	28	41,42

¹These parameters are not well constrained.

References. — (1) Jones & Prosser 1996; (2) Ianna & Schlemmer 1993; (3) Claria, Piatti, & Lapasset 1998; (4) Schneider 1987; (5) Jeffries 1997; (6) Reimers & Koester 1994; (7) Sanders 1973; (8) Maitzen 1993; (9) Claria 1972; (10) Rosvick & VandenBerg 1998; (11) Auner 1974; (12) Lindoff 1972; (13) Sanders 1972; (14) Burkhead 1971; (15) Menzies & Marang 1996; (16) Prosser & Giampapa 1994; (17) Prosser 1993; (18) Sanders & van Altena 1972; (19) Abt, Bolton & Levy, S.G. 1972; (20) Hogg & Kron 1955; (21) Garcia-Pelayo & Alfaro 1984; (22) Barbon & Hassan 1974; (23) Lattanzi, Massone & Munari 1991; (24) Foster *et al.* 2000; (25) Turner 1992; (26) Sanner *et al.* 2000; (27) Marie 1992; (28) Harrington 1992; (29) Tian *et al.* 1998; (30) Galadi-Enriquez, Jordi, Trullols 1998; (31) Mermilliod *et al.* 1996; (32) Becker & Svolopoulos 1976; (33) West 1967; (34) Uggren 1966; (35) Hill & Barnes 1971; (36) Pena & Peniche 1996; (37) Peria & Peniche 1994; (38) Perry, Lee & Barnes 1978; (39) Sagar 1976; (40) Cuffey & McCuskey 1956; (41) Sung & Bessell 1999, (42) Cudworth 1972.

Table 2. Observational Data for CFHT Open Star Clusters

Cluster	V (300/50/10) ¹	B (300/50/10) ¹	R (50/10) ¹	Seeing (") ² (V/B/R)	Air-mass X
NGC 1039 ³ (M34)	1/1/1	1/1/1	1/1	~(0.8/0.75/0.65)	1.18
NGC 2323 ⁴ (M50)	1/1/1	1/1/1	1/1	~(0.85/0.95/0.76)	1.15
NGC 6633	1/1/1	1/1/1	1/1	~(0.6/0.75/0.60)	1.2
NGC 1342	9/1/1	9/1/1	1/1	~(0.81/0.72/0.55)	1.09
NGC 2343	1/1/1	1/1/1	1/1	~(0.87/1.05/0.76)	1.23
NGC 6819 ^{4,5}	9/1/1	9/1/1	1/1	~(0.70/0.89/0.66)	1.1 - 1.65
IC 4665 ³	1/1/1	1/1/1	1/1	~(0.88/1.1/0.96)	1.3 - 1.8
NGC 1778	1/1/1	1/1/1	1/1	~(0.76/0.87/0.74)	1.15
NGC 225	1/1/1	1/1/1	1/1	~(0.82/0.92/0.77)	1.37
STOCK 2 ³	1/1/1	1/1/1	1/1	~(0.78/0.82/0.75)	1.36
NGC 1647 ³	1/1/1	1/1/1	1/1	~(0.65/0.77/0.63)	1.23
NGC 1960 (M36)	1/1/1	1/1/1	1/1	~(0.80/0.82/0.67)	1.05
NGC 2301	1/1/1	1/1/1	1/1	~(0.85/0.88/0.75)	1.37
NGC 1750	1/1/1	1/1/1	1/1	~(0.77/0.93/0.85)	1.20
NGC 2099 ^{4,6} (M37)	3/1/1	3/1/1	1/1	~(0.90/0.82/0.81)	1.03
NGC 7243 ³	1/1/1	1/1/1	1/1	~(0.78/0.79/0.80)	1.16
NGC 2169 ²	2/1/1	2/1/2	2/1	~(1.8/1.8/1.6)	1.06
NGC 2251 ²	2/1/1	2/1/1	1/1	~(1.35/1.30/1.75)	1.37
NGC 2168 ⁴ (M35)	2/1/2	2/1/2	1/1	~(1.35/1.20/0.90)	1.60
Field	V (5/10) ^{1,7}	B (5/10/15/20) ^{1,7}	R (5/10) ^{1,7}		
CALIBRATION SA-92	1/2	2/0/2/0	1/2		
CALIBRATION SA-92	2/2	2/2/0/1	2/2		
CALIBRATION SA-92	0/2	0/0/1/0	0/2		
CALIBRATION SA-95	0/2	0/2/0/0	0/2		
Frame	V Flat Field	B Flat Field	R Flat Field	Bias (Dark Filter)	
PRE-PROCESSING	33	20	9	13	

¹The number of exposures taken in this filter, for each exposure time (sec) listed.

²The data for these clusters suffer from one or more of the following : high humidity, poor focus, or cirrus.

³An equivalent number of blank field images were also obtained for these clusters (offset by 1 degree).

⁴Further reductions are being completed for these clusters. To be published shortly.

⁵Additional 0.2 second and 1.0 second images were obtained at a later date.

⁶Additional 0.5 second images were obtained at a later date.

⁷These images are intentionally taken over a range of air-masses to obtain air-mass terms.

Table 3. Calibration Stars For the 12 CCDs (00-12)

Exposure ¹	Air-mass X	00	01	02	03	04	05	06	07	08	09	10	11
NIGHT 1 – SA-92													
V/5	1.085	0	0	3	1	5	0	1	6	2	1	0	0
B/5	1.101	0	0	3	1	5	0	1	6	3	2	0	0
B/5	1.099	0	0	3	1	5	0	1	6	2	1	0	0
V/10	1.088	0	0	3	1	4	0	1	5	2	0	0	0
V/10	2.105	0	0	3	1	5	0	1	6	2	1	0	0
B/15	1.092	0	0	3	1	5	0	1	6	2	0	0	0
B/15	2.038	0	0	3	1	5	0	1	6	2	0	0	0
NIGHT 2 – SA-92													
B/5	1.519	0	0	3	1	5	0	1	6	3	1	0	0
B/5	1.060	0	0	3	1	5	0	1	6	0	1	0	0
B/10	1.508	0	0	3	1	5	0	1	6	2	1	0	0
B/10	1.060	0	0	3	1	5	0	1	6	2	1	0	0
B/20	1.496	0	0	3	1	5	0	1	6	2	1	0	0
V/5	1.549	0	0	3	1	5	0	1	6	2	1	0	0
V/5	1.059	0	0	3	1	4	0	1	5	2	1	0	0
V/10	1.535	0	0	3	1	5	0	1	5	2	1	0	0
V/10	1.059	0	0	3	1	4	0	0	4	2	1	0	0
NIGHT 2 – SA-95													
B/10	1.389	1	0	0	0	0	0	3	2	4	0	2	0
B/10	1.398	0	0	0	0	0	0	3	2	4	0	2	0
V/10	1.413	1	0	0	0	0	0	3	2	4	0	0	0
V/10	1.422	1	0	0	0	0	0	3	3	4	0	1	0
NIGHT 3² – SA-92													
V/10	1.076	0	0	8	1	5	0	5	8	2	1	0	0
V/10	1.078	0	0	8	1	5	0	5	8	2	1	0	0
B/15	1.081	0	0	8	1	8	0	6	9	2	1	0	0

¹Column organized as filter/exposure time (seconds).

²We used night 1 calibration results to create additional stars for this night.